International Journal of Heat and Technology
Vol. 42, No. 5, October, 2024, pp. 1633-1642
Journal homepage: http://iieta.org/journals/ijht

Comparative Study of Chemically Reacted Nanofluids SWCNT, MWCNT with Modeling of Cattaneo-Christov Heat Fluxes

Bhavanam Naga Lakshmi[1,2*], Varanasi S. Bhagavan[1], Ravuri Mohana Ramana[3], Venkata Ramana Reddy Gurrampati[1]

[1] Department of Engineering Mathematics, Koneru Lakshmaiah Education Foundation, Guntur 522302, India
[2] Department of Mathematics, Vignan Nirula Institute of Engineering and Technology for Women, Guntur 522009, India
[3] Department of Mathematics, Narasaraopet Engineering College (Autonomous), Narasaraopet 522601, India

Corresponding Author Email: hemaevuri29@gmail.com

https://doi.org/10.18280/ijht.420517

Received: 2 August 2024
Revised: 29 September 2024
Accepted: 12 October 2024
Available online: 31 October 2024

Keywords:
Cattaneo-Christov heat flux, SWCNTs, MWCNTs, chemical reaction, mass diffusion

ABSTRACT

This study presents a comparative analysis of chemically reacted nanofluids, specifically single-walled carbon nanotubes (SWCNT) and multi-walled carbon nanotubes (MWCNT), incorporating the advanced modeling of Cattaneo-Christov heat fluxes. It centers on the numerical examination modelling of Cattaneo-Christov heat fluxes to reveal the involvement of carbon nanotubes with the influence of chemical reaction and mass diffusivity of an MHD surface stretching causes nanofluid to flow. A comprehensive assessment is conducted regarding the impact of pertinent limitations on focus. For this, we applied the BVP-4C MATLAB procedure. The investigation includes the development of mathematical models and their numerical solutions to explore the thermal and fluid dynamic behavior of SWCNT and MWCNT nanofluids under chemical reactions. ϕ, M, α, Da, NR, γ, Rc, and Sc are varied to assess their impact on temperature, velocity, and concentration profiles are depicted through graphical representations. The Sherwood and Nusselt numbers and skin friction can also be recognised for practical reasons for numerous estimations of physical parameters. Comparative insights reveal distinct behaviors between SWCNT and MWCNT nanofluids, with SWCNT exhibiting superior thermal conductivity and enhanced heat transfer rates. This model's conclusions are relevant to biological fluids as well as industrial circumstances. These findings agree up to 99.9% with the previous studies and are represented by tabular values.

1. INTRODUCTION

Heat flux could be a vector field condition administering its developmental behavior includes what must be an objective time subsidiary. The vitality condition is defined utilizing Cattaneo-Christov heat fluxes show. The boundary layer influence is anticipated utilizing this demonstration. In specific, numerous research utilize the Fourier Law for the warm flux [1, 2]. Inside the setting of heat convection in a liquid incorporation of Cattaneo laws started with Straughan [3], Cattaneo quantity is elevated sufficient, the convection prepares changes from fixed convection to oscillating convection with more tightly cells, and the warm unwinding impact gets to be considerable. Modelling of Cattaneo - Christov heat fluxes expects the defeat of thermal boundary thickness as related to Fourier law by Ullah et al. [4]. Ahmad et al. [5] demonstrate the Cattaneo-Christov with entropy generation and variable thermal relaxation time is the major focus of the present investigation. Micropolar fluid that absorbs heat with the presence of partial slip and mixed convection is investigated. Reddy et al. [6] deliberated Cattaneo-Christov heat fluxes on heat mass transfers of Casson nanofluid across an improving penetrable regime, using the Soret-Dufour mechanism and thermal radiation. Dadheech et al. [7] see how non-linear chemical reactions across permeable and vertical plates affect entropy formation in Williamson fluid flow and velocity slip. Sarma and Paul [8] the complex behaviour of dusty copper-titanium dioxide and water shear-thickening Carreau hybrid nanofluid flow within a porous vertical cylinder, taking into account the effects of viscous dissipation and the Cattaneo-Christov heat flux model. Sidahmed et al. [9] explained the complex behaviour of dusty copper-titanium dioxide and water shear-thickening Carreau hybrid nanofluid flow within a porous vertical cylinder, taking into account the effects of viscous dissipation and the Cattaneo-Christov heat flux model.

We can raise Incorporating nanoparticles into base fluids improves their thermal conductivity, or particles with a size between one and one hundred nanometers. Even though there are many distinct types of nanoparticles, such as nonmetals (graphite, carbon nanotubes) and metals, oxides, carbides, and nitrides, when it comes to materials that can conduct heat, carbon nanotubes are the most favorable.

A carbon tube having a breadth within the nanometer size is known as a carbon nanotube (CNT) or nanoscale tube. 0.5 to 2.0 nanometer size of single walled carbon nanotubes are

taken. An idealized form of them would set patterns on a two-dimensional graphene regime that have been trundled up into a hollow cylinder. Settled single-wall carbon nanotubes orchestrated in a tube-in-tube arrangement make up multi-walled nano-carbon tubes (MWCNTs). Carbon nanotubes display astonishing features, such as remarkable bendable quality and heat conductivity because of their nano structure and the quality of the connections among carbon particles. The high electrical conductivity is demonstrated by certain SWCNT architectures and other functions such as semiconductors. Furthermore, chemical modifications can be applied to carbon nanotubes. These characteristics are anticipated to be useful in numerous technological fields, including electronics, optics, composite materials which could replace or enhance carbon fibers, nanotechnology, and more material science applications. Sreedevi et al. [10] explained the numerical analysis of heat, mass transfer study of nanofluids with H_2O as base fluid on MHD boundary layer flow having SWCNTs, MWCNTs on a vertical cone implanted over porous medium under suction or/injection and chemical reaction. Asjad et al. [11] scrutinized the Carboxyl methyl cellulose taken as based fluid and Carbon nanotubes as nanoparticles with unsteady MHD viscous fluid flow through inclined plate of infinite length. Moreover, the effects of porosity, MHD, heat source, and chemical reaction are considered. Ullah et al. [12] examines melting impact and entropy study in the flow of hybrid nanomaterials made of motor oil and CNT nanoparticles. A stretched cylinder controls the flow. Jafarimoghaddam et al. [13] considered the Cattaneo-Christov heat fluxes to analyses viscoelastic and second-grade fluid flows with magnetohydrodynamics. Tulu and Ibrahim [14] noticed the flow of MWCNTs-Al_2O_3/engine oil Variable viscous dissipation of mixed convection hybrid nanofluid on rotating cones. Mahabaleshwar et al. [15] investigated that the effect of viscoelastic fluid employed with carbon nanotubes on extending surface on a Darcy permeable media logically underneath an impact of Cattaneo-Christov heat fluxes. Zeeshan et al. [16] deals by steady-state laminar, electrically conducting immiscible flows. In porous media the Newtonian fluid flows between two parallel vertical plates. The medium contains of two regions, engine-oil-based carbon nanotubes (CNTs) is one and the other region is with water. The consequences of nanoparticles of the carbon nanotubes magnetohydrodynamics (MHD) Casson nanofluid flow heat and mass transfer effect by moving vertical plate with a porous region inside an asymmetrical channel is analyzed by Noranuar et al. [17]. And Nazir et al. [18] examines the Maxwell nanofluid is implant with the nanoparticles SWCNTs and MWCNTs. Nanomaterials transformation structure is obtained by utilizing Xue changed theoretical model. Various factors like dissipation, thermal radiations and Ohmic heat influences are adequately implemented in heat formulation. Jaismitha and Sasikumar [19] noticed the radiative viscous dissipation and heat and mass transfer effects interact with the nanoparticles Fe_3O_4, CNTs. Malviya et al. [20] demonstrate that the effect of suction and injection over oscillatory flow of CNT-based hybrid nanofluid along with a channel under the effect of the magnetic field for inspect of heat transfer interpretations. Ramasekhar et al. [21] illustrates the effect of heat transfer boundary layer flow analysis over hybrid nanofluid on an extended cylinder was main focus of the current work. Additionally, the influences of MHD, thermal radiation and porous medium are part of this investigation. Anitha et al. [22] considered the entropy generation investigation of single and multiwall carbon nanotubes flowing in an upright microchannel with varying thermal conductivity. The non-linear thermal radiation and exponential heat source were observed. The micro channel retains convective and no slip boundary conditions. The Buongiorno model was considered in present study. Alharbi et al. [23] differentiate the thermal properties of MHD (magnetohydrodynamic), mono (SWCNTs) and hybrid nanofluids across a bidirectional stretching surface.

The study by Mahabaleshwar et al. [15] investigates innovative use of Cattaneo-Christov heat flux theory in nanofluid flows affected by an inclined magnetic field and a permeable media, focusing on SWCNT/H2O and MWCNT/H_2O nanofluids. The primary goal of the present study is to conduct a comparative analysis of these chemically reacted nanofluids by developing and solving mathematical models to evaluate their thermal and fluid dynamic behaviors. Key parameters like thermal relaxation time, chemical reaction rates, Schmidt number and nanoparticle volume fraction are varied to assess their impact on heat transfer efficiency. Graphical representations illustrate how Cattaneo-Christov heat fluxes affect inclined magnetic flow, analyzing velocity, heat, and mass transfers under various constraints. The findings are pertinent to engineering applications such as radial drives, rotating machinery, viscometers, and aerodynamics. The study also addresses the potential health impacts of carbon nanotubes (CNTs) and their role in enhancing solar collector performance. To ensure consistency, it recommends standardizing the manufacture and evaluation of CNT nanofluids.

This study addresses the lack of comparative analysis between SWCNT and MWCNT nanofluids under the Cattaneo-Christov heat flux model, which accounts for thermal relaxation time. It also explores the effects of chemical reactions on the thermal, concentration and fluid dynamic behaviors of these nanofluids without viscoelasticity, which are not well-documented in existing literature. Furthermore, the impact of varying nanoparticle volume fractions on heat transfer efficiency in chemically reacting nanofluids is thoroughly investigated.

This research introduces a novel comparative analysis of SWCNT and MWCNT nanofluids using Cattaneo-Christov heat flux model, which incorporates thermal relaxation time, providing a more accurate depiction of heat transfer dynamics. It uniquely investigates the interplay of chemical reactions and varying nanoparticle volume fractions on the thermal performance of these nanofluids. Additionally, the study offers new insights into optimizing nanofluid formulations for enhanced thermal management by absence of viscoelasticity that is Newtonian fluid. The present research article endeavors to tackle the subsequent research inquiries:

- How do SWCNT and MWCNT nanofluids compare in terms of thermal conductivity, heat transfer performance when modeled with Cattaneo-Christov heat flux?
- What are the effects of thermal relaxation time on heat transfer characteristics of SWCNT and MWCNT nanofluids?
- How do chemical reactions influence the thermal and fluid dynamic behaviors of these nanofluids?
- What is the impact of varying nanoparticle volume fractions on the efficiency of heat transfer in

chemically reacting SWCNT and MWCNT nanofluids?

2. MATHEMATICAL FORMULATION

This study examines two-dimensional, incompressible flow, which is saturated with SWCNT/MWCNT over a continuously stretched sheet when subjected to an angled magnetic field and a Darcy porous media (see Figure 1). The analysis considers mass diffusion and chemical processes.

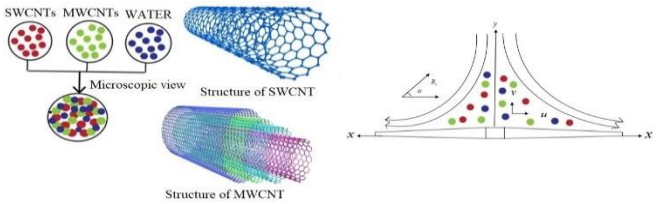

Figure 1. Schematic diagram of flow

The controlling two-dimensional boundary layer flows and the basic equations of this model will be shown in two cases of fluid.

Governing equations [15] are:

$$\frac{\partial u}{\partial x}+\frac{\partial v}{\partial y}=0 \tag{1}$$

$$u\frac{\partial u}{\partial x}+v\frac{\partial v}{\partial y}=\alpha_{nf}\frac{\partial^2 u}{\partial y^2}-\frac{\sigma_{nf}}{\rho_{nf}}B_0^2 u\sin^2(\alpha)-\frac{\nu_{nf}}{K}u. \tag{2}$$

$$\left(\rho C_p\right)_{nf}\left(u\frac{\partial T}{\partial x}+v\frac{\partial T}{\partial y}\right)=-\nabla\left(q+q_r\right). \tag{3}$$

Here *u, v* are horizontal and vertical directions fluid velocities. And *ν, μ, ρ, q, T,* and c_p are the kinematic viscosity, dynamic viscosity, density, heat flux, temperature and specific heat respectively.

The Cattaneo-Christov [15] model can be used to determine

$$q+\lambda\left(\frac{\partial q}{\partial t}+V\nabla q-q\nabla V+\left(\nabla V\right)q\right)=-k\nabla T. \tag{4}$$

where, the heat flow relaxation time λ, and thermal conductivity *k*, are given. When $\lambda = 0$, the basic Fourier's law of heat transport can be reduced from Eq. (4). When *q* is eliminated from Eqs. (3) and (4), we have,

$$\begin{aligned}&u\frac{\partial T}{\partial x}+v\frac{\partial T}{\partial y}+\\&\lambda\left(\begin{aligned}&u\frac{\partial u}{\partial x}\frac{\partial T}{\partial x}+v\frac{\partial v}{\partial y}\frac{\partial T}{\partial y}+u\frac{\partial v}{\partial x}\frac{\partial T}{\partial x}+\\&2uv\frac{\partial^2 T}{\partial x\partial y}+u^2\frac{\partial^2 T}{\partial x^2}+v^2\frac{\partial^2 T}{\partial y^2}\end{aligned}\right)\\&=\alpha_{nf}\frac{\partial^2 T}{\partial y^2}-\frac{1}{\left(\rho C_p\right)_{nf}}\frac{\partial q_r}{\partial y}\end{aligned} \tag{5}$$

$$u\frac{\partial c}{\partial x}+v\frac{\partial c}{\partial y}=D_m\frac{\partial^2 c}{\partial y^2}-K_r\left(c-c_\infty\right) \tag{6}$$

where, D_m is mass diffusion, K_r is chemical reaction.

Considered boundary conditions are [15]:

$$\begin{aligned}&u(x,0)=U_w=cx, v(x,0)=0, u(x,y\to\infty)=0\\&T(x,0)=T_w, T(x,y\to\infty)=T_\infty\\&c\left(x,0\right)=c_w, c(x,y\to\infty)=c_\infty.\end{aligned} \tag{7}$$

Blasius similarity transformations are [15]:

$$\begin{aligned}&u=cxf_\eta(\eta), v=-\sqrt{c\nu_f}\,f(\eta), \theta(\eta)=\frac{T-T_\infty}{T_w-T_\infty},\\&\phi(\eta)=\frac{c-c_\infty}{c_w-c_\infty}, \eta=\sqrt{\frac{c}{\nu_f}}y.\end{aligned} \tag{8}$$

Eq. (1) is met by the foregoing changes and Eqs. (2)-(9) become connected nonlinear differential equations.

$$e_2 f'''+e_1(f.f''-f'^2)-e_3 M\sin^2(\alpha)f'-e_2 Da^{-1}f'=0. \tag{9}$$

$$\left(\frac{K_{hnf}}{K_f}+NR\right)\theta''+e_4\,\mathrm{Pr}\,f\theta'=e_4\gamma(f'\theta'+f^2\theta''). \tag{10}$$

$$(1-\phi)\phi''=Sc(Rc-f\phi'). \tag{11}$$

Boundary conditions related to above equations are:

$$\begin{aligned}&f=0,\ f'=1,\ \theta=1,\ \phi=1,\ \ at\ \eta=0\\&f'\to0,\ \theta\to0,\ \phi\to0\ \ as\ \ \eta\to\infty\end{aligned} \tag{12}$$

where,

$$\begin{aligned}&e_1=\frac{\rho_{nf}}{\rho_f},\ \ e_2=\frac{\mu_{nf}}{\mu_f},\ \ e_3=\frac{\sigma_{nf}}{\sigma_f},\ \ e_4=\frac{\left(\rho C_p\right)_{nf}}{\left(\rho C_p\right)_f},\\&e_5=\frac{k_{nf}}{k_f}.\end{aligned} \tag{13}$$

Mathematically nanofluids constants are defined as by [19]:

$$\begin{aligned}&\upsilon_{nf}=\frac{\mu_{nf}}{\rho_{nf}},\ \ \mu_{nf}=\frac{\mu_f}{(1-\phi)^{2.5}},\\&\rho_{nf}=(1-\phi)\rho_f+\phi\rho_{CNT},\\&\frac{K_{nf}}{K_f}=\frac{1-\phi+2\phi\left(\frac{k_{CNT}}{k_{CNT}-k_f}\right)\ln\left(\frac{k_{CNT}-k_f}{2k_f}\right)}{1-\phi+2\phi\left(\frac{k_f}{k_{CNT}-k_f}\right)\ln\left(\frac{k_{CNT}-k_f}{2k_f}\right)},\\&\left(\rho C_p\right)_{nf}=(1-\phi)\left(\rho C_p\right)_f+\phi\left(\rho C_p\right)_{CNT}.\end{aligned} \tag{14}$$

Here the nondimensional parameters are given by:

$NR = \frac{16\sigma T^3}{3kk^*}$ is the Radiation number.
$Da = \frac{K}{\nu_f}$ is the Darcy number.
$M = \frac{\sigma_f B_0^2}{\rho_f c}$ is Magnetic parameter.
$Pr = \frac{\nu_f}{\alpha_f}$ is Prandtl number.
$\gamma = c\lambda$ is the relaxation time parameter.
$q_r = \frac{-4\sigma^*}{3k^*}\frac{\partial T^4}{\partial y}$ is thermal radiation.
$\alpha_f = \frac{k_f}{(\rho C_p)_f}$ is thermal diffusivity.
$Rc = \frac{k_r(C-C_\infty)}{a}$ is the chemical reaction parameter.

The physical quantities are, "Skin- friction" along x axis C_{fx} "local Nusselt number" Nu_x, "Sherwood number" Sh_x given as:

$$\begin{aligned} Re^{\frac{1}{2}}C_{fx} &= \frac{1}{(1-\phi)^{2.5}}f''(0), \\ Re^{-\frac{1}{2}}Nu_x &= -\frac{K_{nf}}{K_f}\theta'(0), \\ Re^{-\frac{1}{2}}Sh_x &= -\frac{K_{nf}}{K_f}\phi'(0). \end{aligned} \tag{15}$$

where, $Re = \frac{U_w x}{\nu_f}$ is the restricted Reynolds number.

3. NUMERICAL METHOD ALONG WITH VALIDATION

The converted system of nonlinear ODE's (9)-(12) considering boundary conditions in Eqs. (13)-(14) are numerically resolved using MATLAB's BVP-4C solver computational platform. Also, our results are good agreement with earlier outcomes (see Table 2). The procedures below have been done to apply the BVP-4C solution to our solution.

1) For the higher order nonlinear ODE system, more variables are introduced Eqs. (9)-(11).

$$\begin{aligned} b(1) = f, b(2) = f', b(3) = f'', b(4) \\ = \theta, b(5) = \theta', \\ b(6) = \theta'', b(7) = \phi''. \end{aligned}$$

2) Reduce the system of higher order nonlinear ODEs in Eqs. (9)-(10).

$$f' = b(2),$$
$$f'' = b(3),$$
$$f''' = \left(\frac{e_1}{e_2}\right)\left(f'^2 - ff''\right) + \left(\frac{e_3}{e_2}\right),$$
$$\left(M\sin^2\alpha + Da^{-1}\right)f'.$$
$$\theta' = b(5),$$
$$\theta'' = \frac{\Pr e_4}{(e_5 + NR)}\left(-f\theta' + \gamma(f'\theta' + f^2\theta'')\right).$$
$$\phi' = b(7).$$
$$\phi'' = \frac{Sc}{(1-\phi)}\left(R_c\phi - f\theta'\right).$$

3) The attained boundary conditions are:

$$b_0(1) = 0, b_0(2) = 1, b_0(4) = 1, b_0(6) = 1, b_0(7) = 0,$$
$$b_\infty(2) = 0, b_\infty(4) = 0, b_\infty(6) = 0, b_\infty(7) = 0.$$

4) In the bvp4c solver, write the MATLAB code for the system of first-order nonlinear ODEs in Eqs. (9)-(14) and the boundary conditions in Eq. (12) along with the thermophysical properties in Table 1, depict the graphs. The above numerical method is represented as a flow chart in Figure 2.

Table 1. Water and CNT's thermophysical properties

Properties	H_2O (Base Fluid)	SWCNTs	MWCNTs
ρ (kg/m^3)	997.1	425	796
C_p (J/kg. k)	4179	2,600	1,600
k(W/m. k)	0.613	6,600	3,000

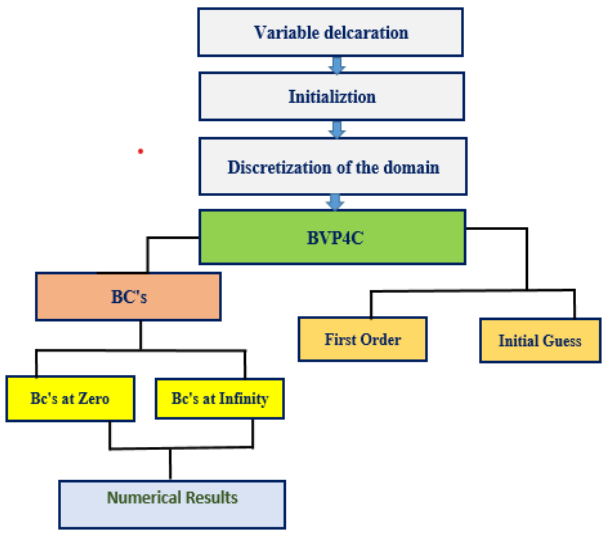

Figure 2. Numerical procedure

Table 2. Comparison of the values of skin friction $-f''(0)$, Nusselt number $-\theta'(0)$ for volume fraction parameter ϕ with previously published work for fixed values $Rc = 0, Sc = 0, \gamma = 0, NR = 0, \alpha = 0, Da = 1, Pr = 0, M = 0$

	$-f''(0)$				$-\theta'(0)$			
ϕ	Sridevi et al. [22]		Current Study		Sridevi et al. [22]		Current Study	
	SWCNT	MWCNT	SWCNT	MWCNT	SWCNT	MWCNT	SWCNT	MWCNT
0.01	0.33901	0.33758	0.33899	0.337586	1.10571	1.07924	1.10582	1.07930
0.1	0.40854	0.39025	0.40853	0.390249	4.80729	4.27816	4.80730	4.27820
0.2	0.50469	0.50484	0.50470	0.504840	12.30352	10.56796	12.30355	10.5678

4. RESULTS AND DISCUSSIONS

The comparative study of the Newtonian, two-dimensional, incompressible, continuously stretched sheet when exposed to a Darcy porous media and an inclined magnetic field. The study considers both mass diffusion and chemical processes. A typical collection of velocity $f'(\eta)$, temperature $\theta(\eta)$, concentration $\theta(\eta)$ distributions for numerous values of the necessary parameters. Non-dimensional parameters ranges are $0.1 \leq \phi \leq 0.4$, $0.1 \leq Rc \leq 0.7$, $0.1 \leq Sc \leq 0.8$, $4 \leq Pr \leq 7$, $1 \leq NR \leq 4$, $-0.02 \leq \gamma \leq 0.01$, $0 \leq \alpha \leq \pi/2$. By fixing other variables as zero for different values of volume fractions we found that there exists a good agreement with the previous literature [10], as represented in Table 2.

The impact of nanoparticle volume fraction (ϕ) on Concentration Profile $\phi(\eta)$ where $(0.1 \leq \phi \leq 0.4)$, through surface regime with coordinate (η) shows in Figure 3. This parameter is analytical in defining the concentration of nanoparticles in a fluid and has a direct impact on its physical characteristics and behaviour. It has been observed from the graph that the concentration profile depreciates as nanoparticle volume fraction (ϕ) values increases due to enhanced interaction among nanoparticles. Higher values of ϕ leads to greater agglomeration and clustering, which reduces the effective diffusivity of the nanoparticles. This causes a decrease in the uniformity of their distribution, resulting in a lower concentration profile.

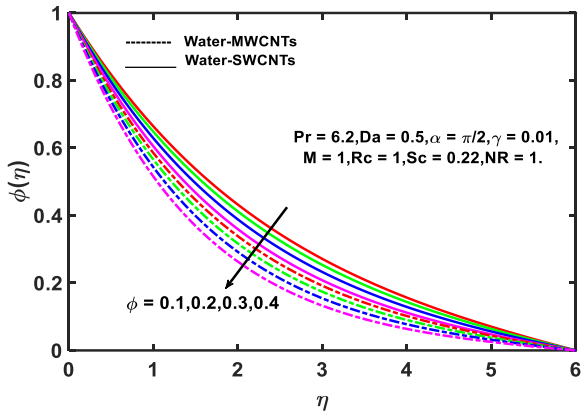

Figure 3. Concentration profile of nanoparticle volume fraction ϕ

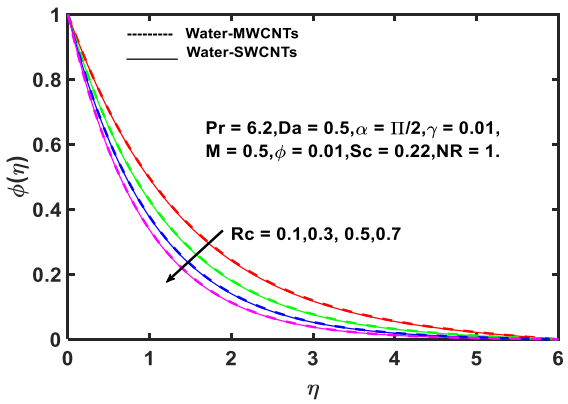

Figure 4. Concentration profile of *Rc*

Figure 4 elucidates chemical reaction effect of on concentration profile $\phi(\eta)$, where on $(0.1 \leq Rc \leq 0.7)$. The chemical reaction parameter (*Rc*) used to describe effect of a chemical reaction on transport properties of a fluid. It usually estimates the rate at which a chemical species interacts within the fluid, which influences the concentration and dispersion of that species. It has been noticed from the graph that concentration profile depreciates as chemical reaction parameter (*Rc*) elevates physically because a higher (*Rc*) indicates a more intense chemical reaction rate. This increased reaction rate accelerates the consumption of nanoparticles, reducing their concentration in the fluid.

Figure 5 illustrates influence of Schmidt number (*Sc*), on concentration profile $\phi(\eta)$ where $0.1 \leq Sc \leq 0.8$, Schmidt number is essential in characterizing relative thickness of velocity boundary layer to mass transfer boundary layer. The concentration profile $\phi(\eta)$ dropped with increasing Schmidt number (*Sc*). Physically, because a greater *Sc* signifies lesser mass diffusivity as compared to momentum diffusivity. This reduced mass diffusivity hampers the dispersion of nanoparticles within the fluid, leading to a steeper concentration gradient and a lower overall concentration profile.

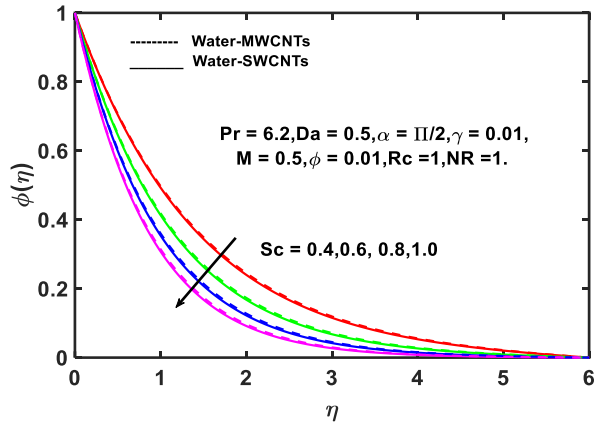

Figure 5. Concentration profile of *Sc*

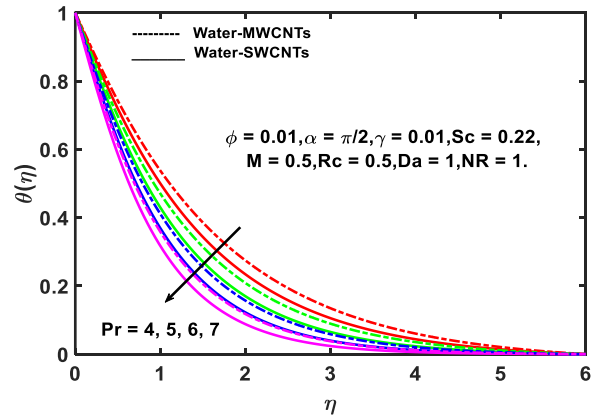

Figure 6. Temperature profile of *Pr*

Figure 6 demonstrates Prandtl number (*Pr*) effect on temperature profile $\theta(\eta)$, where $(4 \leq Pr \leq 7)$, Temperature profile is declining with hiking in (*Pr*), physically because a higher *Pr* signifies a higher momentum diffusivity relative to thermal diffusivity. This means that the fluid's ability to conduct heat is lower compared to its ability to transfer momentum, leading to a thinner thermal boundary layer and thus a steeper temperature gradient. Consequently, the

temperature profile decreases more rapidly. Comparing SWCNT (solid lines) and MWCNT (dashed lines) nanofluids, MWCNTs show a slightly steeper decrease in temperature profiles, suggesting more effective heat transfer. This difference is due to MWCNTs' higher thermal conductivity, which facilitates more efficient heat dissipation compared to SWCNTs.

Figure 7 portrays influence of radiation number (*NR*), on $\theta(\eta)$, where ($1 \le NR \le 4$), through surface regime with coordinate (η). $\theta(\eta)$ is enhance with an increasing radiation number (*NR*), physically because a higher (*NR*) signifies a greater contribution of radiative heat transfer. Radiative heat transfer enhances the overall thermal energy within the system, leading to higher temperatures. Comparing SWCNT and MWCNT nanofluids, SWCNTs (solid lines) generally exhibit a lower temperature profile than MWCNTs (dashed lines) for the same (*NR*) values, indicating that MWCNT nanofluids, with their higher thermal conductivity, respond more significantly to radiative heat transfer, resulting in a more pronounced temperature increase.

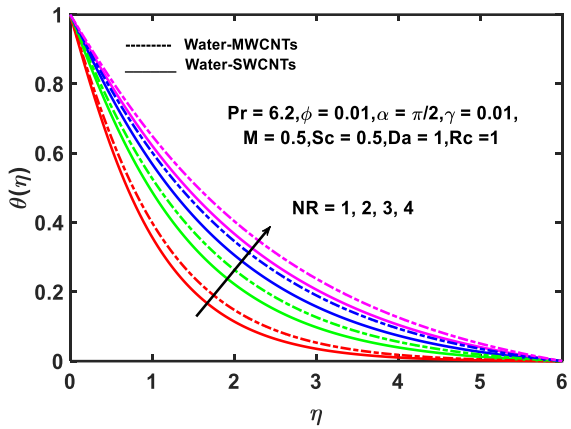

Figure 7. Temperature profile of Radiation number *NR*

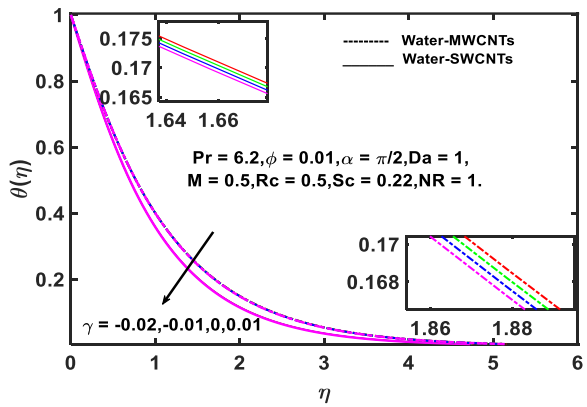

Figure 8. Temperature profile of time relaxation parameter γ

Figure 8 portrays relaxation time parameter (γ), on temperature, where ($-0.02 \le \gamma \le 0.01$). It is particularly relevant in models involving non-Fourier heat conduction, such as the Cattaneo-Christov heat flux model, which accounts for finite speed of thermal propagation. $\theta(\eta)$ lessening with growing in the relaxation time parameter (γ), because a higher γ indicates a delayed response of the material to temperature changes, reducing the overall heat conduction efficiency. This delay causes the heat to dissipate more gradually, resulting in a lower temperature profile. Comparing SWCNT and MWCNT nanofluids, SWCNT show a more pronounced decrease in temperature profiles with increasing (γ), suggesting that SWCNT are more sensitive to the effects of thermal relaxation due to their higher thermal conductivity, which enhances impact of delayed thermal response.

Figure 9 illustrates influence of magnetic inclination angle(α), on the $f'(\eta)$ where ($0 \le \alpha \le \pi/2$), It shows that the enhancement in aligned angle declines the velocity profiles of SWCNTs/H_2O and MWCNTs/H_2O nanofluids. It is frequently owing to the aligned angle, which fortifies magnetic field. Opposing force to the flow owing to the increasing magnetic field, which is called the Lorentz force, this declines thickness. When α=0, magnetic flux has no influence on velocity. However, when α=π/2, the nanofluid particles have the highest resistance.

Figure 10 demonstrates impact of Darcy number (*Da*), velocity profile $f'(\eta)$ where $0.01 \le Da \le 0.04$, $f'(\eta)$ elevates significantly as *Da* values appreciates physically because a higher *Da* indicates higher permeability of the porous medium, allowing fluid to flow more freely. This reduces resistance to fluid motion, resulting in higher velocity profiles. Comparing SWCNT (solid lines) and MWCNT (dashed lines) nanofluids, SWCNTs exhibit a slightly higher velocity profile than MWCNTs for the same (*Da*) values, likely due to SWCNTs' higher thermal conductivity and better dispersion properties, enhancing fluid flow and reducing viscous drag within the medium.

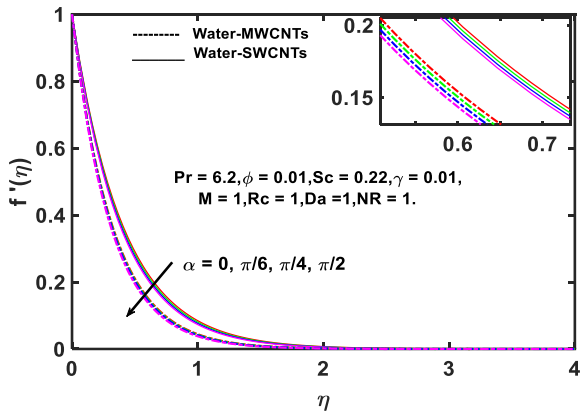

Figure 9. Velocity profile of inclined angle α

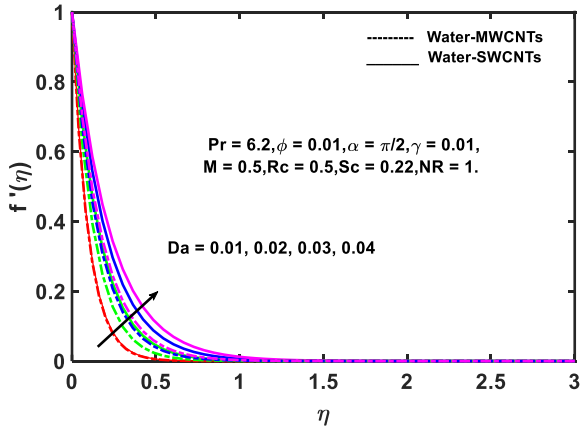

Figure 10. Velocity profile of Darcy number *Da*

Figure 11 emphasis influence of magnetic inclination angle (α), on temperature profile $\theta(\eta)$, where $0 \le \alpha \le \pi/2$. It shows that the enhancement in aligned angle steadily rises the temperature profile $\theta(\eta)$ of SWCNTs/H_2O and

MWCNTs/H_2O nanofluids because a higher values of α enhances the influence of magnetic field on fluid flow, increasing resistive force against the fluid motion. This results in more energy being dissipated as heat within the fluid, raising the temperature profile. Comparing SWCNT and MWCNT nanofluids, SWCNTs show a slightly lower temperature profile than MWCNTs for the same α values. This indicates that MWCNT nanofluids, with their higher thermal conductivity, exhibit a more significant temperature increase due to the combined effects of enhanced thermal energy dissipation and better heat transfer capabilities.

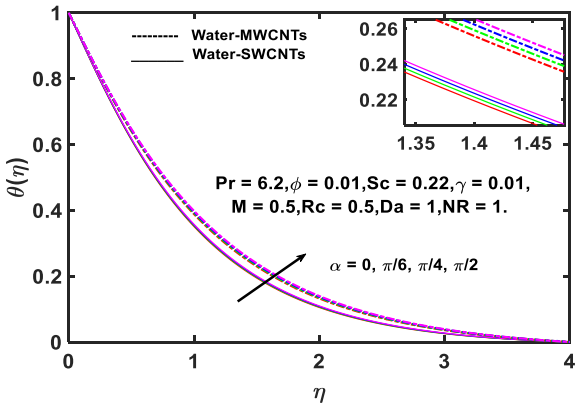

Figure 11. Temperature profile of Inclined angle α

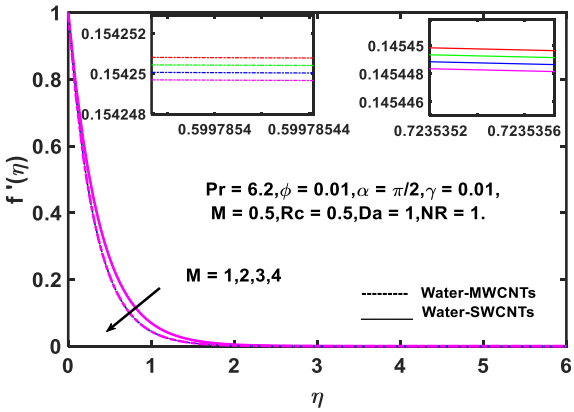

Figure 12. Velocity Profile of Magnetic parameter *M*

The influence of Magnetic parameter M, ($1 \le M \le 4$) on Velocity profile $f'(\eta)$ discussed via Figure 12. The magnetic parameter *M* hikes physically a stronger magnetic field increases Lorentz forces, which act as a drag on the fluid flow. This magnetic drag resists the motion of the fluid, leading to a reduced velocity. Additionally, the increased magnetic field enhances thermal boundary layer, contributing to a further decline in velocity. Moreover, Figure 12 indicates that the velocity of SWCNT nano fluid upsurges more than the velocity of MWCNT nanofluid.

Table 3. Numerical evaluations for skin friction (C_{fx}), Nusselt number (Nu), and Sherwood number (Sh_x) for various values of fluid parameters *Rc, Sc, γ, NR, α, Da, Pr, ϕ* for SWCNT/H_2O

Rc	*Sc*	*γ*	*NR*	*α*	*Da*	*Pr*	*ϕ*	SWCNTs		
								(C_{fx})	(Nu_x)	(Sh_x)
0.1								-2.534742	0.9000437	0.326552
0.3								-2.534742	0.9000437	0.354425
0.5								-2.534742	0.9000437	0.381152
0.7								-2.534742	0.9000437	0.406833
	0.1							-2.534742	0.9000437	0.400269
	0.2							-2.534742	0.9000437	0.521038
	0.4							-2.534742	0.9000437	0.721466
	0.8							-2.534742	0.9000437	1.031189
		-0.02						-2.534742	0.917479	0.543233
		-0.01						-2.534742	0.911772	0.543233
		0.00						-2.534742	0.906092	0.543233
		0.01						-2.534742	0.900437	0.543233
			1					-2.534742	0.900437	0.543233
			2					-2.534742	0.682135	0.543233
			3					-2.534742	0.569191	0.543233
			4					-2.534742	0.501851	0.543233
				0				-2.534737	0.900438	0.543233
				π/6				-2.586313	0.891865	0.542744
				π/4				-2.636880	0.883594	0.542278
				π/2				-2.735213	0.867888	0.541406
					0.01			-10.513177	0.426606	0.519673
					0.02			-7.612497	0.495369	0.523168
					0.03			-6.358028	0.544214	0.525540
					0.04			-5.626875	0.582029	0.527339
						4		-2.534742	0.665153	0.543233
						5		-2.534742	0.773878	0.543233
						6		-2.534742	0.879722	0.543233
						7		-2.534742	0.981610	0.543233
							0.1	-3.216737	0.900437	0.567007
							0.2	-4.318141	0.900437	0.598678
							0.3	-6.029436	0.900437	0.637816
							0.4	-8.864284	0.900437	0.687531

Table 4. Numerical evaluations for skin friction (C_{fx}), Nusselt number (Nu_x), and Sherwood number (Sh_x) for various values of fluid parameters *Rc, Sc, γ, NR, α, Da, Pr, ϕ* for MWCNT/H_2O

Rc	*Sc*	*γ*	*NR*	*α*	*Da*	*Pr*	*ϕ*	MWCNT		
								(C_{fx})	(Nu_x)	(Sh_x)
0.1								-4.058861	0.791562	0.551115
0.3								-5.448607	0.791562	0.581643
0.5								-7.607910	0.791562	0.619387
0.7								-11.184906	0.791562	0.667334
	0.1							-3.198324	0.791562	0.390419
	0.2							-3.198324	0.791562	0.506802
	0.4							-3.198324	0.791562	0.791562
	0.8							-3.198324	0.791562	0.999085
		-0.02						-3.198324	0.805685	0.528197
		-0.01						-3.198324	0.800956	0.528197
		0.00						-3.198324	0.796249	0.528197
		0.01						-3.198324	0.791562	0.528197
			1					-3.198324	0.791562	0.528197
			2					-3.198324	0.600140	0.528197
			3					-3.198324	0.505330	0.528197
			4					-3.198324	0.450006	0.528197
				0				-3.198321	0.777173	0.509488
				π/6				-3.239350	0.771235	0.509205
				π/4				-3.279866	0.765445	0.508931
				π/2				-3.359431	0.754284	0.508408
					0.01			-10.692583	0.348421	0.491073
					0.02			-7.858406	0.422148	0.494321
					0.03			-6.650484	0.472825	0.496450
					0.04			-5.955346	0.510774	0.498016
						4		-3.198324	0.586914	0.528197
						5		-3.198324	0.680077	0.528197
						6		-3.198324	0.773090	0.528197
						7		-3.198324	0.864709	0.528197
							0.1	-4.058861	0.791562	0.551115
							0.2	-5.448607	0.791562	0.581643
							0.3	-7.607910	0.791562	0.619387
							0.4	-11.184906	0.791562	0.667334

The influence of Darcy number (*Da*), on concentration profile $\phi(\eta)$, where ($0.01 \leq Da \leq 0.04$), demonstrated in Figure 13. The concentration profile decreases with increasing Darcy number (*Da*) more for SWCNT than MWCNT due to the higher permeability in SWCNT-based nanofluids. As the Darcy number rises, the porous media becomes more permeable, enhancing fluid flow while decreasing diffusion residence time. For SWCNTs, which have higher surface area and reactivity, this increased permeability accelerates the transport of the chemical species, leading to a steeper decline in concentration compared to MWCNTs.

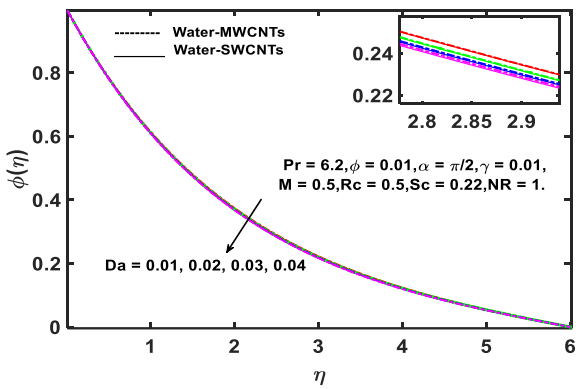

Figure 13. Concentration profile of Darcy number *Da*

In Table 3, it has been observed that for SWCNT/H_2O, *Shx* is enhancing for the parameters *Rc, Sc, Da, ϕ* and diminishes for *α*. For *γ, Da, α* parameters C_{fx} is decreasing, Have no effect for remaining parameters. Also, for time relaxation parameter *γ, NR* shows a substantial decay in (Nu_x).

In Table 4, it was found that for MWCNT/H_2O, *Shx* is growing for the parameters *Rc, Sc, Da, ϕ* and drops for *α*. Also, for time relaxation parameter *γ, α, NR* shows a substantial decay in (Nu_x).

5. CONCLUSIONS

The numerical analysis of two fluids flowing across a stretched surface in the boundary layer, the Cattaneo-Christov model is investigated porosity in CNTs. The relaxation time coefficient is tightly reduced by Prandtl number and the slanted magnetic field. Here are some conclusively monumental findings:

- Temperature and thermal boundary layer thickness are dropped during the increasing γ, *Pr*, hiking for *NR* (Thermal radiation) both nanofluids. Comparatively SWCNTs/H_2O has lessened than MWCNTs/H_2O.
- The thickness of the concentration boundary layer is set off lower for *ϕ*, *Sc*, *Da* and higher to *Rc* for both the nanofluids. More significantly for SWCNT-based nanofluids than for MWCNT-based nanofluids, as higher permeability in SWCNTs.
- As (*M*) increases, the velocity profile decreases further exacerbated by an increased thermal boundary

layer.

- Sh_x is higher in MWCNT/H_2O than SWCNT/H_2O to Sc, Rc. That is with the growing values of Sc and Rc, the mass transfer rate of surface is also enhanced.

6. FUTURE SCOPE

Future research could extend this study to three-dimensional flows and explore more complex fluid models, such as non-Newtonian and hybrid nanofluids. Experimental validation of the numerical results would enhance reliability. Investigating other nanoparticle combinations and base fluids could identify more effective formulations. Optimization techniques could be employed to maximize heat transfer efficiency. Assessing the environmental impact and stability of SWCNT and MWCNT nanofluids in various applications is essential. Finally, applying the findings to real-world engineering problems like solar collectors and cooling systems could demonstrate practical benefits. Studying the influence of additional external forces, such as electric fields or variable magnetic fields, on the behavior of nanofluids could further enhance our understanding of their control and manipulation in advanced engineering systems.

REFERENCES

[1] Ramzan, M., Gul, H., Mursaleen, M., Nisar, K.S., Jamshed, W., Muhammad, T. (2021). Von Karman rotating nanofluid flow with modified Fourier law and variable characteristics in liquid and gas scenarios. Scientific Reports, 11(1): 16442. https://doi.org/10.1038/s41598-021-95644-w

[2] Ahmad Khan, J., Mustafa, M., Hayat, T., Alsaedi, A. (2015). Numerical study of Cattaneo-Christov heat flux model for viscoelastic flow due to an exponentially stretching surface. PLOS one, 10(9): e0137363. https://doi.org/10.1371/journal.pone.0137363

[3] Straughan, B. (2010). Thermal convection with the Cattaneo-Christov model. International Journal of Heat and Mass Transfer, 53(1-3): 95-98. https://doi.org/10.1016/j.ijheatmasstransfer.2009.10.001

[4] Ullah, K.S., Ali, N., Hayat, T., Abbas, Z. (2019). Heat transfer analysis based on Cattaneo-Christov heat flux model and convective boundary conditions for flow over an oscillatory stretching surface. Thermal Science, 23(2 Part A): 443-455. https://doi.org/10.2298/TSCI160225172U

[5] Ahmad, S., Nadeem, S., Muhammad, N., Khan, M.N. (2021). Cattaneo-Christov heat flux model for stagnation point flow of micropolar nanofluid toward a nonlinear stretching surface with slip effects. Journal of Thermal Analysis and Calorimetry, 143: 1187-1199. https://doi.org/10.1007/s10973-020-09504-2

[6] Reddy, K.V., Reddy, G.V.R., Krishna, Y.H. (2021). Effects of Cattaneo-Christov heat flux analysis on heat and mass transport of Casson nanoliquid past an accelerating penetrable plate with thermal radiation and Soret-Dufour mechanism. Heat Transfer, 50(4): 3458-3479. https://doi.org/10.1002/htj.22036

[7] Dadheech, A., Parmar, A., Agrawal, K., Al-Mdallal, Q., Sharma, S. (2022). Second law analysis for MHD slip flow for Williamson fluid over a vertical plate with Cattaneo-Christov heat flux. Case Studies in Thermal Engineering, 33: 101931. https://doi.org/10.1016/j.csite.2022.101931

[8] Sarma, N., Paul, A. (2024). Cattaneo-Christov heat flux effect on Darcy-Forchheimer dual-phase dusty shear-thickening carreau hybrid nanofluid flow along a stretched vertical cylinder. Numerical Heat Transfer, Part B: Fundamentals, 1-25. https://doi.org/10.1080/10407790.2024.2364786

[9] Sidahmed, A.O., Salah, F., Viswanathan, K.K. (2024). Impact of chemical reaction on the Cattaneo-Christov heat flux model for viscoelastic flow over an exponentially stretching sheet. Scientific Reports, 14(1): 16025. https://doi.org/10.1038/s41598-024-65642-9.

[10] Sreedevi, P., Reddy, P.S., Chamkha, A.J. (2018). Magneto-hydrodynamics heat and mass transfer analysis of single and multi-wall carbon nanotubes over vertical cone with convective boundary condition. International Journal of Mechanical Sciences, 135: 646-655. https://doi.org/10.1016/j.ijmecsci.2017.12.007

[11] Asjad, M.I., Aleem, M., Ahmadian, A., Salahshour, S., Ferrara, M. (2020). New trends of fractional modeling and heat and mass transfer investigation of (SWCNTs and MWCNTs)-CMC based nanofluids flow over inclined plate with generalized boundary conditions. Chinese Journal of Physics, 66: 497-516. https://doi.org/10.1016/j.cjph.2020.05.026

[12] Ullah, I., Hayat, T., Alsaedi, A., Fardoun, H.M. (2021). Numerical treatment of melting heat transfer and entropy generation in stagnation point flow of hybrid nanomaterials (SWCNT-MWCNT/engine oil). Modern Physics Letters B, 35(6): 2150102. https://doi.org/10.1142/S0217984921501025

[13] Jafarimoghaddam, A., Turkyilmazoglu, M., Pop, I. (2021). Threshold for the generalized non-Fourier heat flux model: Universal closed form analytic solution. International Communications in Heat and Mass Transfer, 123: 105204. https://doi.org/10.1016/j.icheatmasstransfer.2021.105204

[14] Tulu, A., Ibrahim, W. (2021). Mixed convection hybrid nanofluids flow of MWCNTs-Al_2O_3/engine oil over a spinning cone with variable viscosity and thermal conductivity. Heat Transfer, 50(4): 3776-3799. https://doi.org/10.1002/htj.22051

[15] Mahabaleshwar, U.S., Sneha, K.N., Hatami, M. (2022). Effect of Cattaneo-Christov approximation for viscoelastic fluid with carbon nanotubes on flow and heat transfer. Scientific Reports, 12(1): 9485. https://doi.org/10.1038/s41598-022-13592-5

[16] Zeeshan, A., Shehzad, N., Atif, M., Ellahi, R., Sait, S.M. (2022). Electromagnetic flow of SWCNT/MWCNT suspensions in two immiscible water and engine-oil-based Newtonian fluids through porous media. Symmetry, 14(2): 406. https://doi.org/10.3390/sym14020406

[17] Noranuar, W.N.I.N., Mohamad, A.Q., Shafie, S., Jiann, L.Y. (2023). Heat and mass transfer on Magnetohydrodynamics Casson carbon nanotubes nanofluid flow in an asymmetrical channel via porous medium. Symmetry, 15(4): 946. https://doi.org/10.3390/sym15040946

[18] Nasir, S., Berrouk, A.S., Aamir, A., Shah, Z. (2023). Entropy optimization and heat flux analysis of Maxwell

nanofluid configurated by an exponentially stretching surface with velocity slip. Scientific Reports, 13(1): 2006. https://doi.org/10.1038/s41598-023-29137-3

[19] Jaismitha, B., Sasikumar, J. (2024). Nonlinear dynamics of dissipative water conveying SWCNT/MWCNT/Ferro nanofluid subject to radiation: Thermal analysis by linear slope regression. Numerical Heat Transfer, Part A: Applications, 1-27. https://doi.org/10.1080/10407782.2024.2350027

[20] Malviya, K., Bannihalli Naganagowda, H., Kalluhole Matada, P., Varma, S.V.K., Raju, C.S., Sharma, R. (2024). Heat transfer analysis of MHD oscillatory SWCNT/MWCNT-H2O hybrid nanofluid flow in a channel. ZAMM-Journal of Applied Mathematics and Mechanics/Zeitschrift für Angewandte Mathematik und Mechanik, 104(4): e202300366. https://doi.org/10.1002/zamm.202300366

[21] Ramasekhar, G., Divya, A., Jakeer, S., Reddy, S.R.R., Algehyne, E.A., Jawad, M., Akgül, A., Hassani, M.K. (2024). Heat transfer innovation of engine oil conveying SWCNTs-MWCNTs-TiO2 nanoparticles embedded in a porous stretching cylinder. Scientific Reports, 14(1): 16448. https://doi.org/10.1038/s41598-024-65740-8

[22] Anitha, L., Gireesha, B.J., Keerthi, M.L. (2024). Irreversibility scrutiny of SWCNT and MWCNT nanofluid convective flow using Darcy-Forchheimer rule in an upright microchannel with variable thermal conductivity and Brownian motion and thermophoresis. International Journal of Ambient Energy, 45(1): 2316782. https://doi.org/10.1080/01430750.2024.2316782

[23] Alharbi, K.A.M., Ramzan, M., Shahmir, N., Ghazwani, H.A.S., Elmasry, Y., Eldin, S.M., Bilal, M. (2023). Comparative appraisal of mono and hybrid nanofluid flows comprising carbon nanotubes over a three-dimensional surface impacted by Cattaneo-Christov heat flux. Scientific Reports, 13(1): 7964. https://doi.org/10.1038/s41598-023-34686-8

NOMENCLATURE

M	magnetic numb magnetic numberer
B_0	magnetic field, Tesla
c	constant rate of stretching, s^{-1}
Pr	Prandtl number
NR	radiation number
q	radiative heat flux, $W.m^{-2}$
u, v	velocities, $m.s^{-1}$
T	temperature, K
T_∞	the temperature is far away from the sheet, K
T_w	temperature at the wall, K
k	thermal conductivity

Greek letters

α	thermal diffusivity, $m^2.s^{-1}$
σ_f	electrical conductivity
σ	Stefan Boltzmann constant, $W.m^2K^{-4}$
M	dynamic viscosity, $kg.m^{-1}.\ s^{-1}$
γ	relaxation time parameter.
ν	kinematic viscosity, m^2s^{-1}
ρ	density
η	similarity variable

Subscripts

CNTs	carbon nanotubes
f	base fluid
SWCNTs	single-walled carbon nanotubes
MWCNTs	multi-walled carbon nanotubes